SAND2017-13064J

Experimental Determination of Stability Constant of Ferrous Iron Borate Complex [$FeB(OH)_4^+$] at 25°C from Solubility Measurements

Yongliang Xiong[1], Leslie Kirkes, Jandi Knox, Cassie Marrs, Heather Burton

Sandia National Laboratories (SNL)
Carlsbad Programs Group
4100 National Parks Highway, Carlsbad, NM 88220, USA

[1] Corresponding author, e-mail: yxiong@sandia.gov.

ABSTRACT

In this study, the formation constant ($\log_{10} \beta_1^0$) for $FeB(OH)_4^+$ as expressed in the following reaction,

$$Fe^{2+} + B(OH)_4^- \rightleftharpoons FeB(OH)_4^+$$

is determined as 3.70 ± 0.10 (2σ) at 25°C based on our long-term solubility experiments up to 2,121 days on $Fe(OH)_2$(cr) in the presence of borate ranging from 0.01 to 0.03 mol•kg^{-1}. In our solubility measurements, the equilibrium was attained from the direction of supersaturation. In the experimental design, we used $Fe_2(OH)_3Cl$ (pure iron end member of hibbingite) as the starting material. When $Fe_2(OH)_3Cl$ was in contact with solutions without background concentrations of chloride, it was completely converted to $Fe(OH)_2$(cr).

The stability constant of $FeB(OH)_4^+$ is expected to find applications in many areas of study. For instance, $FeB(OH)_4^+$ may have played an important role in transport of ferrous iron in reducing water bodies at the surface of the primitive Earth. In the near-field of geological repositories, the formation of $FeB(OH)_4^+$ can sequestrate soluble borate, lowering borate concentrations available to the formation of the Am(III)-borate aqueous complex.

1. INTRODUCTION

The formation constant for the ferrous iron borate complex, $FeB(OH)_4^+$, is not known (Bassett, 1980). In a critical review by Bassett (1980), there is a formation constant for the ferric iron borate complex, $FeB(OH)_4^{2+}$, where the oxidation state for iron is +III, but there is no formation constant for $FeB(OH)_4^+$. The species $FeB(OH)_4^+$ is expected to be important in reducing environments. Hence, the presence of $FeB(OH)_4^+$ has relevance for many areas of study.

For instance in the early history of the Earth, before 2.4-2.3 billion years ago (2.4-2.3 Ga), oxygen was poor in the atmosphere (Holland, 1999), and therefore the ocean was anoxic, and iron was present as ferrous iron, i.e., Fe^{2+} (Pufahl and Hiatt, 2012). Based on boron isotope data and geological context, it has been inferred that ancient water bodies, such as oceans, were borate-rich, allowing evaporitic borate precursors to form before 2.1 Ga (e.g., Grew et al., 2011). The aqueous iron-borate complex, $FeB(OH)_4^+$, could have played an important role in transporting iron in ancient, anoxic water bodies.

Another example is in the field of nuclear waste management. Waste containers made of low-carbon steel, and in contact with water, or brine, are expected to corrode, and may develop anoxic conditions, releasing ferrous iron in the near-field of a geological repository. If the brine is in contact with the steel contains borate, ferrous iron in solution can form $FeB(OH)_4^+$. The borate may originate either from the geological formation or from corrosion of borosilicate glass waste forms (possibly used to dispose of high level nuclear waste [HLW]). This iron aqueous complex could be a strong complex and therefore compete with the formation of other borate complexes, sequestering free borate in the system. A good example application is described below for the Waste

55 Isolation Pilot Plant (WIPP), a U.S. DOE geological repository for defense-related
56 transuranic (TRU) waste in the bedded salt formations in New Mexico, USA.
57 Borate can form aqueous complexes with Nd(III) and Eu(III) (Borkowski et al.,
58 2010; Schott et al., 2014, 2015), analogs for actinides in the +III oxidation state, such as
59 Am(III). If borate were to form an aqueous complex with Am(III) in the WIPP
60 repository, complexation with borate would contribute to the mobility of Am(III).
61 Complexation of Am(III) with borate would also increase the solubility of Am(III). The
62 inventory of Am(III) in waste was 143 kg for the WIPP Compliance Application Re-Certification
63 in 2009 (CRA-2009). The borate concentrations in the two WIPP brines that are important for
64 assessing performance of the repository, i.e., Generic Weep Brine (GWB), and Energy
65 Research and Development Administration (WIPP Well) 6 (ERDA-6), are 0.180 mol•kg^{-1} and
66 0.0692 mol•kg^{-1} (Xiong and Lord, 2008), respectively. Thus, the potential for formation of an
67 Am(III)/borate complex exists and sequestration of free borate in the $FeB(OH)_4^+$ complex
68 in WIPP should be evaluated. The stability constant for the $FeB(OH)_4^+$ complex is
69 needed for the evaluation.
70 The objective of this study is to determine the stability constant for $FeB(OH)_4^+$
71 via solubility measurements. The goal is two-fold: (1) to provide a quantitative tool to
72 assess the role of $FeB(OH)_4^+$ in transportation of iron in the surface environments of the
73 primitive Earth, and (2) to determine the stability constant for $FeB(OH)_4^+$ to use in
74 assessment of performance of geological repositories .
75
76 2. EXPERIMENTAL METHODS
77 In our experimental design, we used $Fe_2(OH)_3Cl$ as the starting material. As was
78 previously observed in our laboratory, if $Fe_2(OH)_3Cl$ is added to a solution with zero

79 background Cl- concentration, then solid phase $Fe(OH)_2$ forms. We considered that this
80 design, using the phase transformation, approaches the equilibrium from the direction of
81 supersaturation. The supporting solutions used were 0.01, 0.02, and 0.03 $mol \cdot kg^{-1}$ H_3BO_3,
82 as polyborate ions may form when total boron concentrations are higher than 0.03
83 $mol \cdot kg^{-1}$ (Mesmer et al., 1972). If polyborate ions are present, they will complicate data
84 interpretations. To prevent the problem of polyborate ions from our experiments, the
85 borate concentrations did not exceed 0.03 $mol \cdot kg^{-1}$ in our experimental design.
86 All experiments, including synthesizing the starting material and preparing
87 supporting solutions, were conducted in a VAC® glovebox (Model: Omni-Lab) with an
88 anoxic control system. Anoxic conditions were maintained using a source gas of 5 % H_2
89 (balance Ar) and O_2 scrubber boxes manufactured by VAC®. The oxygen concentration
90 within the glovebox was maintained below 1 ppm, routinely around 0.2 ppm. Prior to
91 preparing solutions, deionized water (DI) with 18.3 MΩ was sparged with the anoxic-
92 glovebox gas in the glovebox for a minimum of one hour.
93
94 2.1 Synthesis of Starting Material
95 In our synthesis of the starting material, $Fe_2(OH)_3Cl$, we followed a method
96 similar to that used in our laboratory before, as described in Nemer et al. (2011). In the
97 synthesis, we first dissolved 48 grams of $FeCl_2 \cdot 4H_2O(s)$ (Fisher Scientific, ACS grade)
98 into 100 mL degassed DI water. Second, we dissolved 41 grams of NaOH(s) (Fisher
99 Scientific, ACS grade) into 60 mL degassed DI water. Third, 26 mL of the NaOH
100 solution described above was transferred into the $FeCl_2$ solution described above by using
101 a graduated cylinder. Then, 26 mL of degassed water was used to rinse the graduated

cylinder used in the previous step. The rinsed solution was also transferred into the above $FeCl_2$ solution. Finally, the plastic bottle containing the $FeCl_2$ solution was doubly wrapped with Teflon tape, first on the thread, and then on the lid. We shook the bottle well before storing it. After some time (in this case, about a year), the precipitate was filtered out.

In the filtration process based on gravity, after the filter paper and filtering apparatus was set-up, the slurry containing the precipitate was poured into the filtering apparatus, and the bottle was rinsed thoroughly with DI water until the bottle was clear. The rinsing DI water was also poured into the filtering apparatus. The solid was washed several times. The slurry was left on the filtering apparatus for a few days to ensure that the solid was completely filtered and to allow drying of the solid. In the filtration process, we tried two types of filter papers. We first used #40 Whatman® filter paper. However, the filtrate looked cloudy after filtration for two hours. Therefore, the filtrate was collected and poured back into the filtering apparatus to make sure that no $Fe_2(OH)_3Cl$ was lost. Then we used Millipore-Isopore® membrane 1.2 μm filter paper. This filter paper was better, as the filtrate was very clear.

2.2 Experimental Setup

Supersaturation experiments using the phase transformation from $Fe_2(OH)_3Cl(cr)$ to $Fe(OH)_2(cr)$, mentioned before, are conducted at 25.0 ± 0.5 C. In our solubility experiments, approximately 1.5 grams of $Fe_2(OH)_3Cl(cr)$ were placed into serum bottles along with 100 mL of supporting solutions with the desired borate concentrations. The supporting solutions consisted of 0.01, 0.02, and 0.03 $mol \cdot kg^{-1}$ H_3BO_3. All supporting

125 solutions were prepared from ACS grade H_3BO_3 from Fisher Scientific, and deaerated DI
126 water.

127 Solution samples were periodically withdrawn from the experiments to determine
128 if the system had reached equilibrium. Before each sampling, pH readings were taken for
129 each experiment. In each sampling, about 3 mL of solution samples were taken from
130 each experiment, and the solution samples were filtered through a 0.2 μm filter, and
131 transferred into pre-weighed 10 mL Grade A volumetric flasks. After filtration, masses
132 of each solution sample were determined with a balance precise to the fourth decimal
133 place. Samples were then immediately acidified with 0.5 mL of the Optima® Grade
134 HNO_3 from Fisher Scientific, and diluted to 10 mL with DI water. Prior to chemical
135 analyses for iron and boron using the PerkinElmer Optima 3300 Dual View (DV) or
136 PerkinElmer Optima 8300 Dual View (DV) ICP-AES, aliquots from the afore-mentioned
137 acidified samples were further diluted to an appropriate ionic strength.

138 The pH readings were measured with an Orion-Ross combination pH glass
139 electrode, coupled with an Orion Research EA 940 pH meter that was calibrated with
140 three pH buffers (pH 4, pH 7, and pH 10). The pH scale used in this work is the
141 concentration scale (Mesmer and Holmes, 1992), denoted as pH_m.

142 Chloride concentrations were determined with a DIONEX ion chromatograph
143 (IC) (DIONEX IC 3000) with a conductivity detector.

144 The final measurements for this study included iron, chloride, boron, and
145 hydrogen ion molal concentration data.

146 Solid phases were analyzed using a Bruker D8 Advance X-ray diffractometer
147 with a Sol-X detector, before and after experiments. XRD patterns were collected using
148 CuKα radiation at a scanning rate of 1.33^o/min for a 2θ range of 10–90^o.
149
150 3. RESULTS
151 Experimental results are tabulated in Table 1. In Figure 1, the XRD patterns are
152 presented. In the lower portion of Figure 1, it is shown that the starting material is
153 $Fe_2(OH)_3Cl$ with a minor amount of $Fe(OH)_2$(cr). In the upper portion of Figure 1, the
154 XRD patterns for the solids after experiment are displayed. These XRD patterns indicate
155 the complete transformation from $Fe_2(OH)_3Cl$ to $Fe(OH)_2$(cr), demonstrating that
156 $Fe(OH)_2$(cr) was the solubility-controlling phase.
157 In Figure 2, negative logarithms of hydrogen ion concentrations (pH_m) as a
158 function of experimental time are shown. For the purpose of comparison with a similar
159 system on brucite [$Mg(OH)_2$(cr)], the evolution of pH_m in a long-term experiment
160 approaching equilibrium with brucite from supersaturation (Xiong, 2008) is also
161 displayed in Figure 2. The trends are similar for both systems. In the case of brucite, the
162 reversal, i.e., the results from the experiment approaching equilibrium from the direction
163 of supersaturation being the same with the results from the direction of undersaturation,
164 was attained at ~83 days (Xiong, 2008). The experiments from both directions were
165 conducted in that work. In the case of $Fe(OH)_2$(cr), it seems that the steady state was
166 attained starting from, or after, the second sampling (i.e., 108 days, see Table 1), when
167 the evolution of iron concentrations and the solubility quotients as a function of
168 experimental time described below are taken into consideration.

In Figure 3, molalities of dissolved ferrous iron as a function of experimental time are presented. It shows that the iron concentrations in the first sampling (i.e., 37 days) are much higher than those in the rest of the samplings, indicating that the system was still oversaturated with respect to $Fe(OH)_2$(cr). This is similar to the evolution of magnesium concentrations and solubility products.

In Figure 4, the solubility quotients in logarithmic units are plotted versus experimental time. In the pH_m range of our experiments, Fe^{2+} is the dominant species. The dissolution reaction for $Fe(OH)_2$(cr) can be generally expressed as follows,

$$Fe(OH)_2(cr) + 2H^+ \rightleftharpoons Fe^{2+} + 2H_2O(l) \quad (1)$$

$$Q = \frac{m_{\Sigma Fe(II)}}{(m_{H^+})^2} \quad (2)$$

Figure 4 shows that the steady state was attained starting from the second or third sampling. In our previous work on $Fe(OH)_2$(cr) from the direction of undersaturation, the steady state was attained no later than 94 days (Nemer et al. 2011). Combining this work on $Fe(OH)_2$(cr) from supersaturation in the presence of borate with our previous work on $Fe(OH)_2$(cr) from undersaturation without borate, we infer that the reversal for the solubility of $Fe(OH)_2$(cr) was attained in ~100-200 days. This time scale is similar to that for the solubility of brucite, which attained the reversal at ~83 days (Xiong, 2008).

4. THERMODYNAMIC MODEL, DISCUSSIONS, AND APPLICATIONS

191

192 4.1 Thermodynamic Modeling

193 In the hydrolysis speciation scheme for Fe(II) recommended by Baes and Mesmer
194 (1976), Fe^{2+} is dominant at pH ≤ 9, followed by $FeOH^+$ at 9 < pH ≤ 10.5, by $Fe(OH)_3^-$ at
195 pH > 10.5. $Fe(OH)_2(aq)$ and $Fe(OH)_4^{2-}$ are weak species, and they do not have their
196 dominant fields (Baes and Mesmer, 1976). The formation of $FeOH^+$ can be expressed as,

197

198 $$Fe^{2+} + H_2O(l) \rightleftharpoons FeOH^+ + H^+ \quad (3)$$

199

200 $$K_{1,1}^0 = \frac{(m_{H^+}) \times (m_{FeOH^+})}{m_{Fe^{2+}}} \times \frac{(\gamma_{H^+}) \times (\gamma_{FeOH^+})}{\gamma_{Fe^{2+}}} \quad (4)$$

201

202 where m_i is a molal concentration for the i-th species, γ_i an activity coefficient for the i-th
203 species.

204 In the presence of borate, $FeB(OH)_4^+$ can form according to the following
205 reaction,

206

207 $$Fe^{2+} + B(OH)_4^- \rightleftharpoons FeB(OH)_4^+ \quad (5)$$

208

209 $$\beta_1^0 = \frac{m_{FeB(OH)_4^+}}{(m_{Fe^{2+}}) \times (m_{B(OH)_4^-})} \times \frac{\gamma_{FeB(OH)_4^+}}{(\gamma_{Fe^{2+}}) \times (\gamma_{B(OH)_4^-})} \quad (6)$$

210

211 Therefore, the iron species considered in this study for modeling include Fe^{2+},
212 $FeOH^+$ and $FeB(OH)_4^+$, according to the experimental pH_m's in this work.
213 Based on our experimental data, we model the equilibrium constant at infinite
214 dilution for Reaction (5). In the modeling, we use the computer code EQ3/6 Version 8.0a
215 (Wolery et al. 2010; Xiong 2011) as a modeling platform. The essence of the modeling is
216 to minimize the difference between experimental and model predicted values. The
217 EQ3/6 code has been successfully used as a modeling platform in a number of previous
218 studies at ambient temperature (e.g., Xu et al., 1999; Kong et al., 2013; Xiong et al.
219 2013a, 2013b, 2017; Xiong 2015) and at elevated temperatures up to 523.15 K (Xiong
220 2013a, 2013b, 2014).
221 Experimental data after attainment of the steady state are selected for the
222 modeling. Those data are used to generate EQ3/6 input files in the first step. In the
223 second step, the values of the targeted parameter (e.g., $\log_{10} \beta_1^0$) are changed until the
224 difference between experimental values (e.g., $m_{\Sigma Fe(II)}$) and model-produced values
225 predicted by the computer code is minimized. In the third step, the final selected value
226 for the targeted parameter is verified to see how it reproduces experimental data.
227 The database used for the modeling is DATA0.FM2 (Xiong and Domski, 2016),
228 which utilizes the Pitzer model for calculations of activity coefficients of aqueous
229 species. The original borate chemistry in DATA0.FM2 was from Felmy and Weare
230 (1986), with updates from Xiong et al. (2013). The equilibrium constant for Reaction (1)
231 is from Nemer et al. (2011) and its recent revision (Domski, 2017), and the first
232 hydrolysis constant for Reaction (3) is from the EQ3/6 database, DATA0.YMP (Wolery
233 and Jarek, 2003).

234 Based on the modeling, the equilibrium constant for Reaction (5) is determined to
235 be 3.70 ± 0.10 (2σ) in 10-based logarithmic units (Table 2). In Figure 5, the model-
236 predicted solubilities of $Fe(OH)_2$(cr) in the presence of borate at 0.01, 0.02, and 0.03
237 mol•kg^{-1} are compared with the experimental values. Two things are clear from Figure
238 5. First, solubilities of $Fe(OH)_2$(cr) in the presence of borate are much higher than those
239 without borate, suggesting that borate forms an aqueous complex, $FeB(OH)_4^+$, with Fe(II)
240 to enhance solubilities of $Fe(OH)_2$(cr). Second, Figure 5 demonstrates that the values
241 predicted using the model with $FeB(OH)_4^+$ are in good agreement with the experimental
242 values.
243 Van den Berg (1984) determined the equilibrium constants for $CuB(OH)_4^+$ and
244 $PbB(OH)_4^+$ at 25ºC and I = 0.7 mol•dm^{-3} KNO_3 as 3.48 and 2.2 in 10-based logarithmic
245 units, respectively. When these conditional equilibrium constants are extrapolated to
246 infinite dilution using the B dot equation (Helgeson, 1969), they are 4.19 and 2.91,
247 respectively. In the extrapolation to infinite dilution, the ionic strength on a molar scale
248 is converted to one (i.e., 0.72 mol•kg^{-1}) on a molal scale by using the density equation for
249 KNO_3 from Sőhnel and Novotný (1985). Therefore, the strength of $FeB(OH)_4^+$ is
250 between those for $CuB(OH)_4^+$ and $PbB(OH)_4^+$.
251
252 4.2 Applications
253 Before the Great Oxidation Event (GOE) that happened before 2.4-2.3 Ga, the
254 partial pressure of oxygen, P_{O_2}, was lower than 10^{-4} atm in the Earth's atmosphere
255 (Bekker and Holland, 2012). Under such reducing conditions, dissolved iron was present
256 as ferrous iron in the primitive oceans (Pufahl and Hiatt, 2012). Under the pH conditions

257 of the primitive oceans that was close to neutral, but slightly alkaline, $FeB(OH)_4^+$ may
258 have played an important role in transport of iron at the surface of the primitive Earth, as
259 borate is expected to be present in the primitive oceans at significant concentrations to
260 have formed evaporitic borate precursors (e.g., Grew et al., 2011).

261 The only competitor for $FeB(OH)_4^+$ in transport of iron in the primitive oceans
262 may have been $FeHCO_3^+$. The formation of $FeHCO_3^+$ can be expressed as follows,
263

264 $$Fe^{2+} + HCO_3^- \rightleftharpoons FeHCO_3^+ \quad (7)$$

265

266 The equilibrium constant for Reaction (7) is 2.72 in 10-based logarithmic units (Mattigod
267 and Sposito, 1979). In comparison with $\log_{10} \beta_1^0$ of 3.70 ± 0.10 (2σ) for $FeB(OH)_4^+$, the
268 iron complex with bicarbonate is weaker. Therefore, $FeB(OH)_4^+$ may have played a
269 dominant role in transport of iron in the primitive oceans.

270 In geological repositories for disposal of nuclear waste, iron is present in
271 repositories as waste containers and waste, and borate concentrations from the geological
272 formations and degradation of borosilicate waste forms for high level nuclear waste
273 (HLW) can be significant. For instance, tincalconite ($Na_2B_4O_7 \cdot 5H_2O$) has been observed as
274 one corrosion product for borosilicate glass for HLW under repository conditions in China
275 (Zhang et al., 2012). The formation of tincalconite suggests that the borate concentrations are
276 high enough to reach the saturation limit of tincalconite. As borate can form a complex with
277 Am(III), $AmHB_4O_7^{2+}$ (Borkowski et al., 2010; Xiong, 2017), the formation of such a Am(III)-
278 borate complex could contribute to the higher solubility of Am(III). However, under the reducing

conditions of geological repositories, the formation of $FeB(OH)_4^+$ will alleviate the effect of borate complexation with Am(III).

5. SUMMARY

In this work, we determine the stability constant of $FeB(OH)_4^+$ based on solubility measurements on $Fe(OH)_2$(cr) in the presence of borate. The strength of this complex is between those for $CuB(OH)_4^+$ and $PbB(OH)_4^+$. It is expected that $FeB(OH)_4^+$ plays an important role under reducing environments for iron chemistry.

6. ACNOWLEDGEMENTS

Sandia National Laboratories is a multi-mission laboratory operated by National Technology and Engineering Solutions of Sandia, LLC., a wholly owned subsidiary of Honeywell International, Inc., for the U.S. Department of Energy's National Nuclear Security Administration under contract DE-NA-0003525. This research is funded by WIPP programs administered by the Office of Environmental Management (EM) of the U.S Department of Energy. We are grateful to Diana Goulding, Brittany Hoard, Danelle Morrill, Mathew Stroble, and Kira Vincent, for their laboratory assistance.

298 REFERENCES
299
300 Aja, S.U., Wood, S.A. and Williams-Jones, A.E., 1995. The aqueous geochemistry of Zr
301 and the solubility of some Zr-bearing minerals. *Applied Geochemistry*, *10*(6),
302 pp.603-620.

303 Baes, C. F., Jr., and Mesmer, R. E. (1976) The Hydrolysis of Cations, John Wiley, New
304 York.

305 Bassett, R.L., 1980. A critical evaluation of the thermodynamic data for boron ions, ion
306 pairs, complexes, and polyanions in aqueous solution at 298.15 K and 1 bar.
307 Geochimica et Cosmochimica Acta, **44**, 1151–1160.

308 Bekker, A. and Holland, H.D., 2012. Oxygen overshoot and recovery during the early
309 Paleoproterozoic. *Earth and Planetary Science Letters*, *317*, pp.295-304.

310 M. Borkowski, M. Richmann, D.T. Reed, and Y.-L. Xiong, Y.-L., Radiochimica Acta 98, 577
311 (2010).

312 Domski, P., 2017. "Memo AP-155, Task 2 EQ3/6 Database Update". Memo to the
313 Record Center. Carlsbad, NM. Sandia National Laboratories.

314 Felmy, A.R., and Weare, J.H. (1986) The prediction of borate mineral equilibria in
315 natural waters: Applications to Searles Lake, California. Geochimica et
316 Cosmochimica Acta, 50, 2771–2783.

317 Grew, E.S., Bada, J.L. and Hazen, R.M., 2011. Borate minerals and origin of the RNA
318 world. *Origins of Life and Evolution of Biospheres*, *41*(4), pp.307-316.

319 Helgeson, H.C., 1969. Thermodynamics of hydrothermal systems at elevated
320 temperatures and pressures. *American journal of science*, *267*(7), pp.729-804.

321 Holland, H.D., 1999. When did the Earth's atmosphere become oxic? A reply. *Geochem.*
322 *News*, *100*, pp.20-22.

323 Kong, X.Z., Tutolo, B.M. and Saar, M.O., 2013. DBCreate: A SUPCRT92-based
324 program for producing EQ3/6, TOUGHREACT, and GWB thermodynamic
325 databases at user-defined T and P. *Computers & geosciences*, *51*, pp.415-417.

326 Mattigod, S.V., and Sposito, G., 1979, Chemical modeling of trace metal equilibria in
327 contaminated soil solutions using the computer program GEOCHEM, in Jenne, E.A.,
328 ed., Chemical Modeling in Aqueous Systems: Speciation, Sorption, Solubility, and
329 Kinetics: Amer. Chem. Soc., Washington, 837-856.

330 Mesmer, R.E. and Holmes, H.F., 1992. pH, definition and measurement at high
331 temperatures. *Journal of solution chemistry*, *21*(8), pp.725-744.

Mesmer, R.E., Baes, C. F. JR., and Sweeton, F. H., 1972, Acidity measurements at elevated temperatures. VI. Boric acid equilibria. Inorganic Chemistry, **11**, 537–543.

Nemer, M.B., Xiong, Y., Ismail, A.E. and Jang, J.H., 2011. Solubility of Fe 2 (OH) 3 Cl (pure-iron end-member of hibbingite) in NaCl and Na 2 SO 4 brines. *Chemical Geology*, *280*(1), pp.26-32.

Pufahl, P.K. and Hiatt, E.E., 2012. Oxygenation of the Earth's atmosphere–ocean system: a review of physical and chemical sedimentologic responses. *Marine and Petroleum Geology*, *32*(1), pp.1-20.

J. Schott, J. Kretzschmar, M. Acker, S. Eidner, M.U. Kumke, B. Drobot, A. Barkleit, S. Taut, V. Brendler, and T. Stumpf, T., Dalton Transactions 43, 11516 (2014).

J. Schott, J. Kretzschmar, S. Tsushima, B. Drobot, M. Acker, A. Barkleit, S. Taut, V. Brendler, and T. Stumpf, T., Dalton Transactions 44, 11095 (2015).

Sőhnel, O, Novotný, P., 1985, Densities of aqueous solutions of inroganic substances. Elsevier, New York, 335 p.

U.S. Department of Energy (DOE) (1996) Title 40 CFR Part 191 Compliance Certification Application for the Waste Isolation Pilot Plant (October). 21 vols. DOE/CAO-1996-2184. Carlsbad, NM: Carlsbad Area Office.

U.S. Department of Energy (DOE) (2004) Title 40 CFR Part 191 Compliance Recertification Application for the Waste Isolation Pilot Plant, Vol. 1-8. DOE/WIPP 2004-3231. Carlsbad, NM: U.S. Department of Energy Carlsbad Field Office.

U.S. Department of Energy (DOE) (2009) Title 40 CFR Part 191 Compliance Recertification Application for the Waste Isolation Pilot Plant. DOE/WIPP 2009-3424. Carlsbad, NM: US DOE Waste Isolation Pilot Plant, Carlsbad Field Office.

Van den Berg, C.M., 1984. Determination of the complexing capacity and conditional stability constants of complexes of copper (II) with natural organic ligands in seawater by cathodic stripping voltammetry of copper-catechol complex ions. *Marine Chemistry*, *15*(1), pp.1-18.

Wolery, T.J., Jarek, R.L., 2003. Software user's manual EQ3/6 (version 8.0). Sandia National Laboratories, Albuquerque/New Mexico.

Wolery, T.J., Xiong, Y.-L., and Long, J. (2010) Verification and Validation Plan/Validation Document for EQ3/6 Version 8.0a for Actinide Chemistry, Document Version 8.10. Carlsbad, NM: Sandia National laboratories. ERMS 550239.

Wood, S.A., D.A. Palmer, D.J. Wesolowski, and P. Bénézeth (2002) The aqueous geochemistry of the rare earth elements and yttrium. Part XI. The solubility of

367 $Nd(OH)_3$ and hydrolysis of Nd^{3+} from 30 to 290 °C at saturated water vapor pressure
368 with in-situ pH_m measurement. In Hellmann, R. and Wood, S.A., ed., Water-Rock
369 Interactions, Ore Deposits, and Environmental Geochemistry: A Tribute to David
370 Crerar, Special Publication 7, The Geochemical Society, pp. 229–256.

371 Xiong, Y.-L. (2008) Thermodynamic properties of brucite determined by solubility
372 studies and their significance to nuclear waste isolation. Aquatic Geochemistry, 14,
373 223–238.

374 Xiong, Y.-L. (2011) WIPP Verification and Validation Plan/Validation Document for
375 EQ3/6 Version 8.0a for Actinide Chemistry, Revision 1, Document Version 8.20.
376 Supersedes ERMS 550239. Carlsbad, NM. Sandia National Laboratories. ERMS
377 555358.

378 Xiong, Y.-L. (2013a) An aqueous thermodynamic model for solubility of potassium
379 ferrate in alkaline solutions to high ionic strengths at 283.15 K to 333.15 K. Journal
380 of Solution Chemistry, 42, 1393–1403.

381 Xiong, Y.-L. (2013b) A thermodynamic model for silica and aluminum in alkaline
382 solutions with high ionic strength at elevated temperatures up to 100 °C :
383 Applications to zeolites. American Mineralogist, 98, 141–153.

384 Xiong, Y.-L. (2014) A Pitzer model for the Na-$Al(OH)_4$-Cl-OH system and solubility of
385 boehmite (AlOOH) to high ionic strength and to 250°C. Chemical Geology, 373,
386 37–49.

387 Xiong, Y.-L. (2015) Experimental determination of lead carbonate solubility at high ionic
388 strengths: a Pitzer model description. Monatshefte für Chemie-Chemical Monthly,
389 146, 1433–1443.

390 Xiong, Y., 2017. Solution Chemistry for Actinide Borate Species to High Ionic Strengths:
391 Equilibrium Constants for $AmHB_4O_7^{2+}$ And $AmB_9O_{13}(OH)_4$(cr) and Their
392 Importance to Nuclear Waste Management. *MRS Advances*, *2*(13), pp.741-746.

393 Xiong, Y.-L., and Lord, A.S. (2008) Experimental investigations of the reaction path in
394 the $MgO–H_2O–CO_2$ system in solutions with various ionic strengths, and their
395 applications to nuclear waste isolation. Applied Geochemistry, 23, 1634–1659.

396 Xiong, Y.-L., Domski, P.S., 2016. "Updating the WIPP Thermodynamic Database,
397 Revision 1, Supersedes ERMS 565730." Carlsbad, NM: Sandia National
398 Laboratories. ERMS 566047.

399 Xiong, Y.-L., Deng, H.-R., Nemer, M., and Johnsen, S. (2010a) Experimental
400 determination of the solubility constant for magnesium chloride hydroxide hydrate
401 ($Mg_3Cl(OH)_5·4H_2O$), phase 5) at room temperature, and its importance to nuclear

waste isolation in geological repositories in salt formations. Geochimica et Cosmochimica Acta, 74, 4605-4611.

Xiong, Y.-L., Kirkes, L., and Westfall, T., (2013a) Experimental Determination of Solubilities of Sodium Tetraborate (Borax) in NaCl Solutions, and A Thermodynamic Model for the Na–$B(OH)_3$–Cl–SO_4 System to High Ionic Strengths at 25 °C. American Mineralogist, 98, 2030–2036.

Xiong, Y.-L., Kirkes, L., Westfall, T., and Roselle, R. (2013b) Experimental determination of solubilities of lead oxalate (PbC_2O_4(cr)) in a NaCl medium to high ionic strengths, and the importance of lead oxalate in low temperature environments. Chemical Geology, 342, 128–137.

Xu, T., Pruess, K. and Brimhall, G., 1999. An improved equilibrium-kinetics speciation algorithm for redox reactions in variably saturated subsurface flow systems. *Computers & Geosciences*, *25*(6), pp.655-666.

Zhang, Z., Gan, X., Wang, L. and Xing, H., 2012. Alteration Development of the Simulated HLW Glass at High Temperature in Beishan Underground Water. *International Journal of Corrosion*, *2012*

420
421 Table 1. Experimental results produced in this study at 25.0 ± 0.5°C.
422

Experimental Number	Supporting Medium, H_3BO_3, molal	Experimental time, days	pH	Molality of total dissolved ferrous iron, $m_{\Sigma Fe(II)}$
FeB(OH)4-0.01B-1	0.01	37	7.88	1.24E-02
FeB(OH)4-0.01B-2	0.01	37	7.88	1.16E-02
FeB(OH)4-0.02B-1	0.02	37	7.94	8.49E-03
FeB(OH)4-0.02B-2	0.02	37	7.95	8.75E-03
FeB(OH)4-0.03B-1	0.03	37	8.02	7.60E-03
FeB(OH)4-0.03B-2	0.03	37	8.03	7.38E-03
FeB(OH)4-0.01B-1	0.01	108	7.97	4.01E-03
FeB(OH)4-0.01B-2	0.01	108	7.96	7.84E-03
FeB(OH)4-0.02B-1	0.02	108	8.00	7.30E-03
FeB(OH)4-0.02B-2	0.02	108	8.08	5.65E-03
FeB(OH)4-0.03B-1	0.03	108	8.11	6.10E-03
FeB(OH)4-0.03B-2	0.03	108	8.12	6.55E-03
FeB(OH)4-0.01B-1	0.01	184	7.83	5.20E-03
FeB(OH)4-0.01B-2	0.01	184	7.95	3.84E-03
FeB(OH)4-0.02B-1	0.02	184	7.95	4.78E-03
FeB(OH)4-0.02B-2	0.02	184	7.94	3.61E-03
FeB(OH)4-0.03B-1	0.03	184	7.97	4.44E-03
FeB(OH)4-0.03B-2	0.03	184	8.04	2.75E-03
FeB(OH)4-0.01B-1	0.01	457	7.87	6.59E-03
FeB(OH)4-0.01B-2	0.01	457	7.88	4.95E-03
FeB(OH)4-0.02B-1	0.02	457	7.94	6.25E-03
FeB(OH)4-0.02B-2	0.02	457	7.94	3.87E-03
FeB(OH)4-0.03B-1	0.03	457	7.96	6.09E-03
FeB(OH)4-0.03B-2	0.03	457	7.98	5.12E-03
FeB(OH)4-0.01B-1	0.01	496	7.84	6.82E-03
FeB(OH)4-0.01B-2	0.01	496	7.83	5.12E-03
FeB(OH)4-0.02B-1	0.02	496	7.85	6.55E-03
FeB(OH)4-0.02B-2	0.02	496	7.84	4.07E-03
FeB(OH)4-0.03B-1	0.03	496	7.67	6.41E-03
FeB(OH)4-0.03B-2	0.03	496	7.90	5.24E-03

FeB(OH)4-0.01B-1	0.01	576	7.85	6.85E-03
FeB(OH)4-0.01B-2	0.01	576	7.85	5.10E-03
FeB(OH)4-0.02B-1	0.02	576	7.88	6.71E-03
FeB(OH)4-0.02B-2	0.02	576	7.88	4.03E-03
FeB(OH)4-0.03B-1	0.03	576	7.88	6.40E-03
FeB(OH)4-0.03B-2	0.03	576	7.90	5.38E-03
FeB(OH)4-0.01B-1	0.01	616	7.77	6.83E-03
FeB(OH)4-0.01B-2	0.01	616	7.80	5.22E-03
FeB(OH)4-0.02B-1	0.02	616	7.83	6.62E-03
FeB(OH)4-0.02B-2	0.02	616	7.82	3.94E-03
FeB(OH)4-0.03B-1	0.03	616	7.85	6.26E-03
FeB(OH)4-0.03B-2	0.03	616	7.87	5.36E-03
FeB(OH)4-0.01B-1	0.01	1547	7.73	7.54E-03
FeB(OH)4-0.01B-2	0.01	1547	7.78	5.48E-03
FeB(OH)4-0.02B-1	0.02	1547	7.80	7.29E-03
FeB(OH)4-0.02B-2	0.02	1547	7.86	3.33E-03
FeB(OH)4-0.03B-1	0.03	1547	7.82	7.22E-03
FeB(OH)4-0.03B-2	0.03	1547	7.81	6.28E-03
FeB(OH)4-0.01B-1	0.01	1617	7.75	7.78E-03
FeB(OH)4-0.01B-2	0.01	1617	7.80	5.42E-03
FeB(OH)4-0.02B-1	0.02	1617	7.82	7.26E-03
FeB(OH)4-0.02B-2	0.02	1617	7.90	3.31E-03
FeB(OH)4-0.03B-1	0.03	1617	7.82	7.20E-03
FeB(OH)4-0.03B-2	0.03	1617	7.83	6.30E-03
FeB(OH)4-0.01B-1	0.01	1743	7.70	7.82E-03
FeB(OH)4-0.01B-2	0.01	1743	7.78	5.37E-03
FeB(OH)4-0.02B-1	0.02	1743	7.81	7.19E-03
FeB(OH)4-0.02B-2	0.02	1743	7.88	3.19E-03
FeB(OH)4-0.03B-1	0.03	1743	7.80	7.16E-03
FeB(OH)4-0.03B-2	0.03	1743	7.81	6.28E-03
FeB(OH)4-0.01B-1	0.01	1841	7.80	8.11E-03
FeB(OH)4-0.01B-2	0.01	1841	7.81	5.46E-03
FeB(OH)4-0.02B-1	0.02	1841	7.91	7.74E-03
FeB(OH)4-0.02B-2	0.02	1841	7.89	3.34E-03

FeB(OH)4-0.03B-1	0.03	1841	7.85	7.69E-03
FeB(OH)4-0.03B-2	0.03	1841	7.90	6.78E-03
FeB(OH)4-0.01B-1	0.01	1868	7.76	8.30E-03
FeB(OH)4-0.01B-2	0.01	1868	7.81	5.43E-03
FeB(OH)4-0.02B-1	0.02	1868	7.84	7.60E-03
FeB(OH)4-0.02B-2	0.02	1868	7.92	3.20E-03
FeB(OH)4-0.03B-1	0.03	1868	7.81	7.57E-03
FeB(OH)4-0.03B-2	0.03	1868	7.82	6.63E-03
FeB(OH)4-0.01B-1	0.01	2024	7.69	8.29E-03
FeB(OH)4-0.01B-2	0.01	2024	7.77	5.26E-03
FeB(OH)4-0.02B-1	0.02	2024	7.76	7.79E-03
FeB(OH)4-0.02B-2	0.02	2024	7.89	3.11E-03
FeB(OH)4-0.03B-1	0.03	2024	7.77	7.74E-03
FeB(OH)4-0.03B-2	0.03	2024	7.78	6.74E-03
FeB(OH)4-0.01B-1	0.01	2121	7.70	8.15E-03
FeB(OH)4-0.01B-2	0.01	2121	7.78	4.96E-03
FeB(OH)4-0.02B-1	0.02	2121	7.76	7.25E-03
FeB(OH)4-0.02B-2	0.02	2121	7.86	2.95E-03
FeB(OH)4-0.03B-1	0.03	2121	7.75	7.54E-03
FeB(OH)4-0.03B-2	0.03	2121	7.74	6.83E-03

423
424

Table 2. The equilibrium constants for the system Fe^{2+}—OH^-—$B(OH)_4^-$ at 25°C

Reactions	$\log_{10} K^0$	Reference
$Fe(OH)_2(cr) + 2H^+ \rightleftharpoons Fe^{2+} + 2H_2O(l)$	12.89 ± 0.13 (2σ)	Nemer et al. (2011), Domski (2017)
$Fe^{2+} + H_2O(l) \rightleftharpoons FeOH^+ + H^+$	–9.3148	DATA0.YMP*
$Fe^{2+} + B(OH)_4^- \rightleftharpoons FeB(OH)_4^+$	3.70 ± 0.10 (2σ)	This Study

* Wolery and Jarek (2003)

Figure Captions

Figure 1. The XRD pattern for a representative sample after experiments is displayed. An XRD pattern for the synthetic $Fe(OH)_2$(cr) produced in this work with the reference standard of $Fe(OH)_2$(cr) from PDF-4+ 2016 (Software Version 4.16.04, Database Version 4.1605) of the International Center for Diffraction Data (ICDD) is also presented.

Figure 2. A plot showing hydrogen ion concentrations on a molal scale (pH_m) measured by this study as a function of experimental time.

Figure 3. A plot showing Fe(II) concentrations as a function of experimental time.

Figure 4. A plot showing *log Q* as a function of experimental time

Figure 5. Comparisons of experimental solubilities of $Fe(OH)_2$(cr) in the presence of borate with the solubilities of $Fe(OH)_2$(cr) predicted by using models with $FeB(OH)_4^+$ and without $FeB(OH)_4^+$, as a function of hydrogen ion concentrations on a molal scale.

460

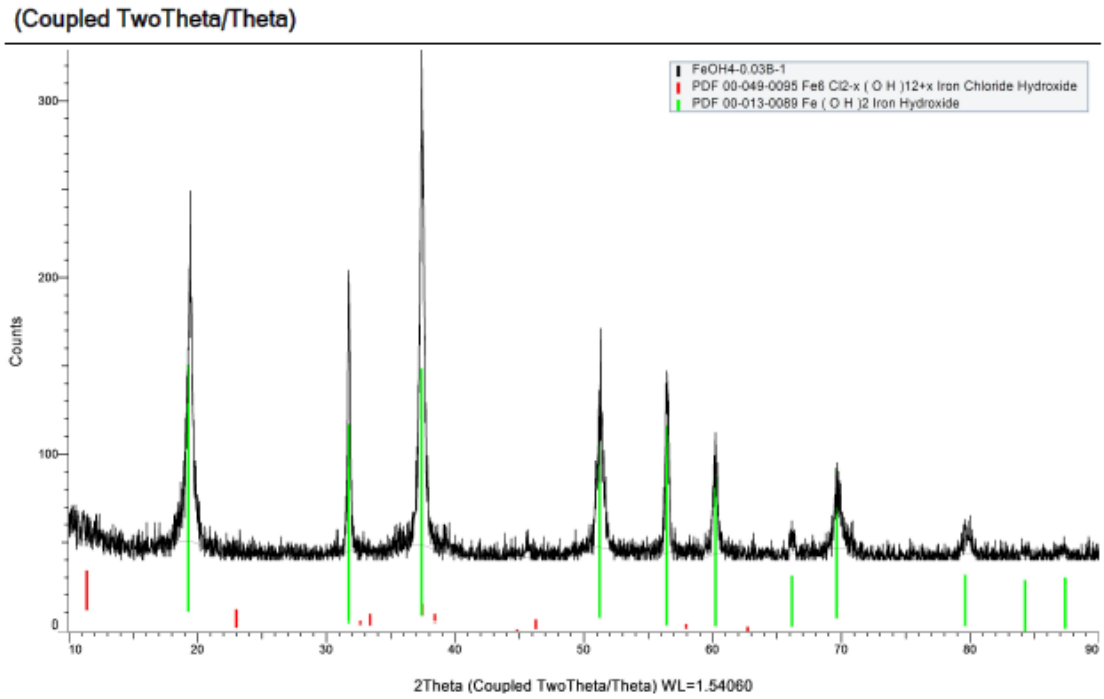

461
462
463 Figure 1.
464
465

466

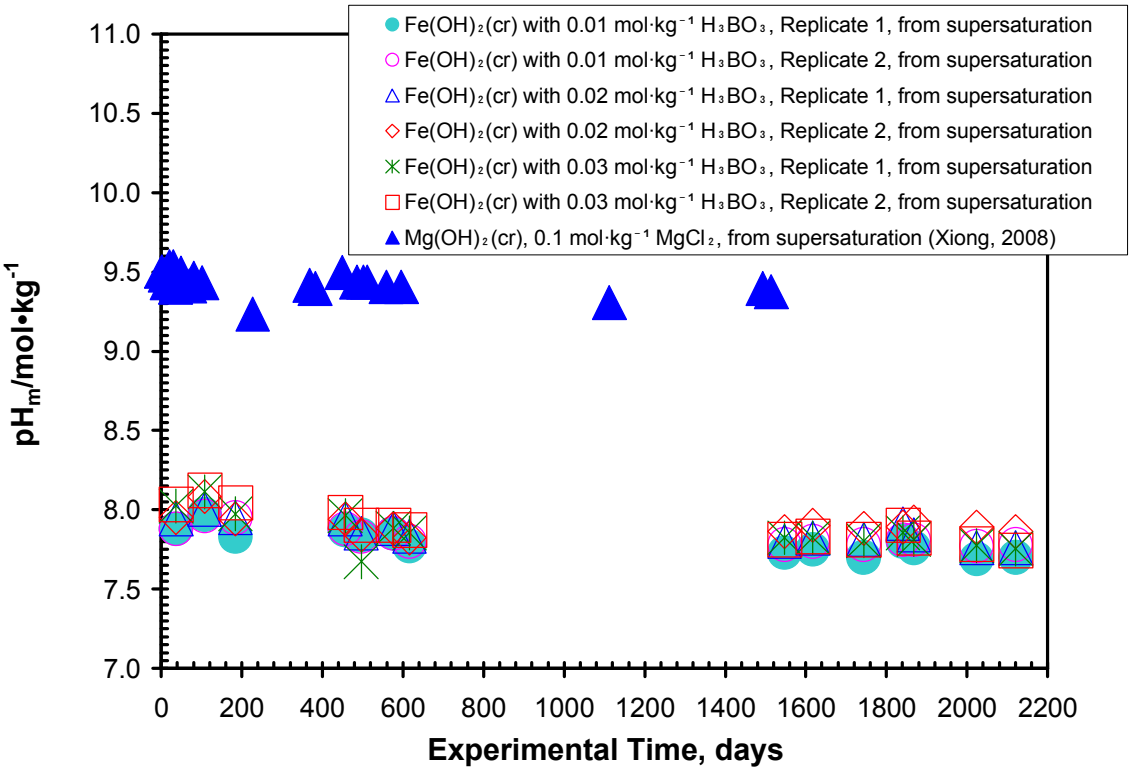

467
468 Figure 2.
469

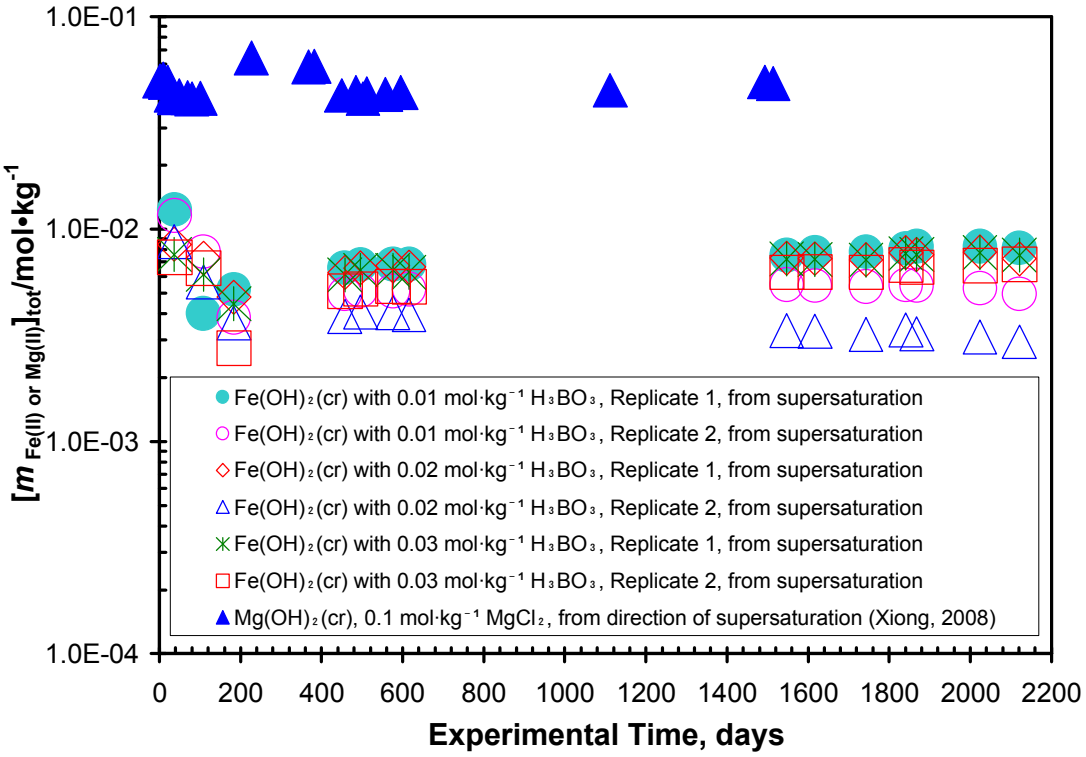
1.0E-01
1.0E-02
1.0E-03
1.0E-04
[m Fe(II) or Mg(II)]tot/mol•kg-1
0
200
400
600
800
1000
1200
1400
1600
1800
2000
2200
Experimental Time, days
Fe(OH)2(cr) with 0.01 mol·kg-1 H3BO3, Replicate 1, from supersaturation
Fe(OH)2(cr) with 0.01 mol·kg-1 H3BO3, Replicate 2, from supersaturation
Fe(OH)2(cr) with 0.02 mol·kg-1 H3BO3, Replicate 1, from supersaturation
Fe(OH)2(cr) with 0.02 mol·kg-1 H3BO3, Replicate 2, from supersaturation
Fe(OH)2(cr) with 0.03 mol·kg-1 H3BO3, Replicate 1, from supersaturation
Fe(OH)2(cr) with 0.03 mol·kg-1 H3BO3, Replicate 2, from supersaturation
Mg(OH)2(cr), 0.1 mol·kg-1 MgCl2, from direction of supersaturation (Xiong, 2008)

Figure 3.

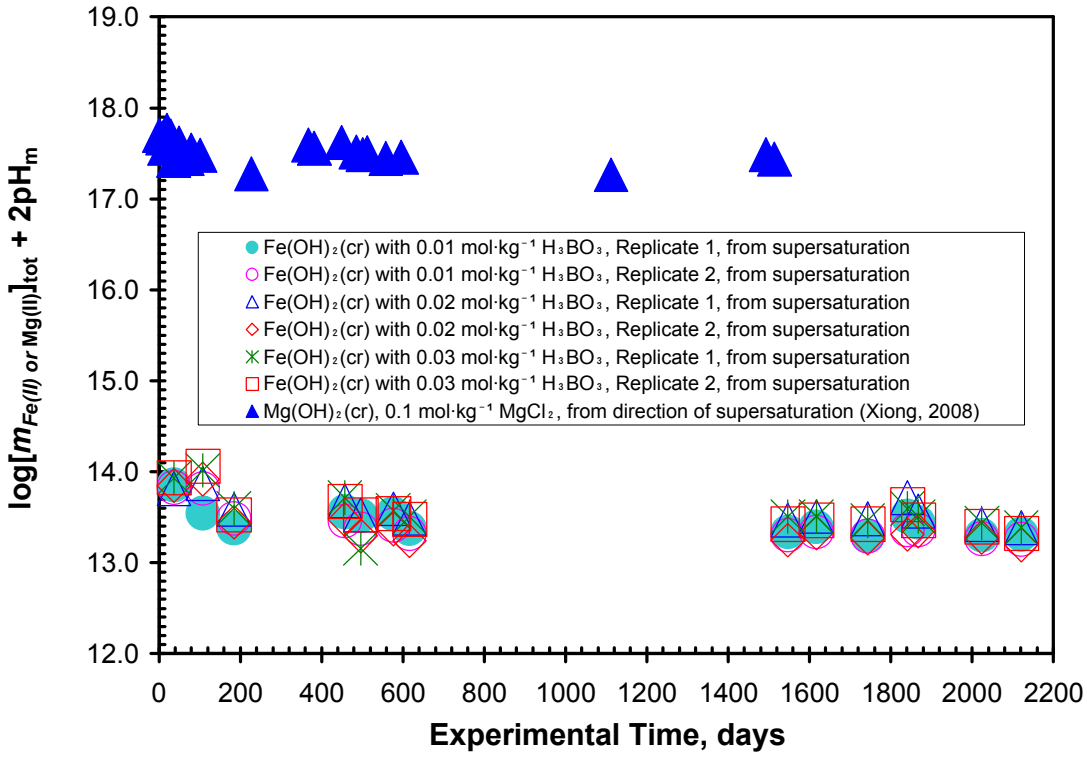

475
476 Figure 4.
477

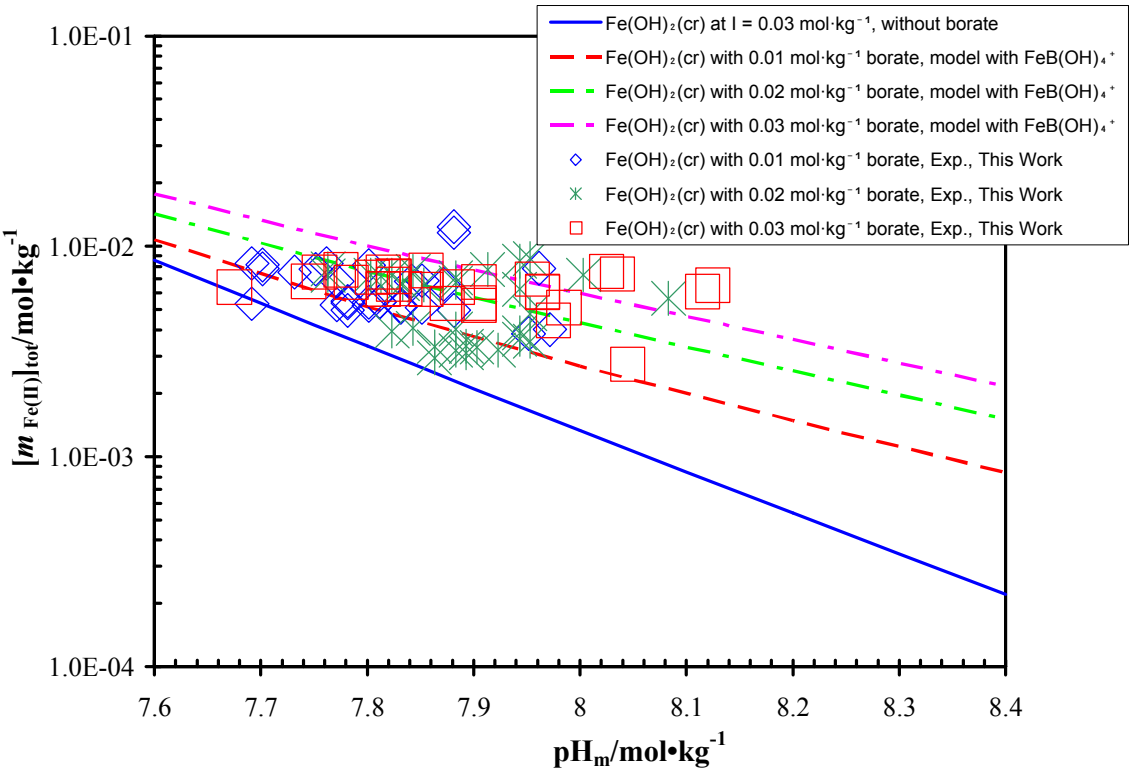
Fe(OH)₂(cr) at I = 0.03 mol·kg⁻¹, without borate
Fe(OH)₂(cr) with 0.01 mol·kg⁻¹ borate, model with FeB(OH)₄⁺
Fe(OH)₂(cr) with 0.02 mol·kg⁻¹ borate, model with FeB(OH)₄⁺
Fe(OH)₂(cr) with 0.03 mol·kg⁻¹ borate, model with FeB(OH)₄⁺
Fe(OH)₂(cr) with 0.01 mol·kg⁻¹ borate, Exp., This Work
Fe(OH)₂(cr) with 0.02 mol·kg⁻¹ borate, Exp., This Work
Fe(OH)₂(cr) with 0.03 mol·kg⁻¹ borate, Exp., This Work
1.0E-01
1.0E-02
1.0E-03
1.0E-04
[m Fe(II)]tot/mol•kg-1
7.6
7.7
7.8
7.9
8
8.1
8.2
8.3
8.4
pHm/mol•kg-1

Figure 5.